MDCT in Neurovascular Imaging

Birgit Ertl-Wagner, Dominik Morhard

Institute of Clinical Radiology, University of Munich, Grosshadern Campus, Munich, Germany

Background

In the early 1990s, the first spiral computed tomography (CT) scanners, consisting of only one detector row, were introduced. With the advent of multidetector-row CT scanners (MDCTs) in 1998, larger scan volumes and an improved longitudinal resolution at a shorter scanning time were achieved by simultaneous acquisition of multiple slices per gantry rotation. The acquisition of volume data using the spiral scanning technique was a ground-breaking step in the development of CT. With volume data sets it became possible, for the first time, to reconstruct images in any orientation along the patient axis [1, 2], thus enabling applications like CT angiography (CTA) and revolutionizing non-invasive assessment [3]. Also, three-dimensional reformations, such as multi-planar reformations (MPR), maximum-intensity projections (MIP), volume-rendering technique (VRT), and surface-rendering technique (SRT) could be attained from volume data sets [4].

In 2004, 32- to 64-slice CT systems were introduced, establishing neurovascular CTA examinations in submillimeter resolution and thereby enabling isotropic reformations and acquisitions in a strict arterial phase [5-7].

The first dual-source-CT was installed in 2006. The device's two tubes and orthogonally mounted detectors enabled the acquisition of one axial image by a gantry rotation of 90° instead of the 180° of single-source scanners. This cut acquisition time in half – an important factor especially in cardiac imaging [8]. The two tubes can also be run at different voltages – the so-called dual-energy-CT-mode, e.g., at 140 and 80 kV – in order to obtain different attenuations for material decomposition [9]. This approach can also be used for selective bone-removal or iodine quantification without motion artifacts or misregistrations.

In addition to the fast-paced innovations of new scanners, new developments in post-processing with semi-automatic quantifications of stenoses or bone-removal techniques have had a pronounced influence on current clinical routine [10, 11]. Modern neurovascular CTA as a non-invasive imaging modality is replacing conventional diagnostic digital subtraction angiography (DSA) with increasing frequency [12-14].

Protocol Parameters for Neurovascular MDCT

As there are numerous different MDCT systems on the market, a multitude of optimized scanning protocols are available for neurovascular imaging, depending on the chosen system. Sample protocols for non-enhanced CT (NECT) and CTA are listed in Tables 1, and 2, respectively [15].

If the patient is to undergo purely intracranial CT, it should be kept in mind that most of the latest MDCT systems do not allow the gantry to be tilted for spiral scanning. Therefore, the only way to keep the radiation-sensitive lenses of the eyes out of the path of the radiation beam is by correcting the patient's position (Fig. 1).

In addition, it needs to be considered that spiral CT scanning, especially using scanners with a low number of detectors, always includes a short area of over-beaming, i.e., radiation exposure at the beginning and end of the imaging scan range that exceeds that of the scan range, and an area of over-ranging that is needed to obtain additional data required for

(e-ISBN 978-88-470-0802-1 Springer-Verlag Milan Berlin Heidelberg New York). Published online at www.mdct.net

Table 1. Scan parameters: non-enhanced cranial computed tomography (CT)

Parameters	4- to 8-detector-row scanners	10- to 20-detector row scanners	32- to 64-detector-row scanners
Scanner protocol			
Tube voltage (kV)	120	120	120
Rotation time (s)	0.75	1.0	1.0
Tube current time product (mAs)	190–250 CDTIvol < 60	190–250 CDTIvol < 60	350 CDTIvol < 60
Collimation (mm)	2.5	1.5	0.6
Normalized pitch	0.65–0.85	0.65–0.85	0.85
Scan range	Sagittal suture to foramen magnum		
Scan direction	Craniocaudal		
Reconstruction settings			
Slice increment (mm)	Whole-brain reconstructions: 5 or Split reconstructions: supratentorial: 8, and infratentorial: 3		
Slice thickness (mm)	Whole-brain reconstructions: 5 or Split reconstructions: supratentorial: 8 and infratentorial: 3		
Kernel	Standard		

Table 2. Scan parameters: computed tomography angiography (CTA)

Parameters	4- to 8-detector-row scanners	10- to 20-detector-row scanners	32- to 64-detector-row scanners	Dual-energy scanners
Scanner protocol				
Tube voltage (kV)	120	120	120	Tube A: 140 Tube B: 80
Rotation time (s)	0.5	0.33–0.5	0.33	0.33
Tube-current time product (mAs)	135–200	135–200	135–240	Tube A: 55 Tube B: 230
Collimation (mm)	1–1.25	0.6–0.75	0.6	0.6
Normalized pitch	0.9–1	0.9–1	0.9–1.2	1.0
Scan range	Intracranial scans: sagittal suture to foramen magnum Scans including extracranial vasculature: aortic arch to sagittal suture			
Scan direction	Caudocranial	Craniocaudal for standard scans in a late arterial phase, caudocranial for scanning in an explicit, very early arterial phase (e.g., aneurysm visualization in therapy planning)		
Reconstruction settings				
Slice increment (mm)	1	0.6	0.4–0.5	0.4–0.5
Slice thickness (mm)	1.25	0.75–1	0.6–0.75	0.6–0.75
Kernel	Standard CTA kernel for cross-sectional MPR and MIP (e.g., H_20 for Siemens scanners), using softer kernels (e.g., H31 for Siemens scanners) for VRT or SRT reconstructions can provide more convenient results.			
Contrast-agent injection protocol				
Concentration (mg iodine/ml)	300–400			
Volume (ml)	80–120	80–100	80–100	80–100
Injection rate (ml/s)	3–4, monophasic injection			
Saline pusher (ml; ml/s)	30; 3.0			
Delay (s)	Automatic bolus detection at aortic arch plus 3–6s, if available; if not available, 20s for strict intracranial scans, 12–15s for scans including extracranial vasculature			

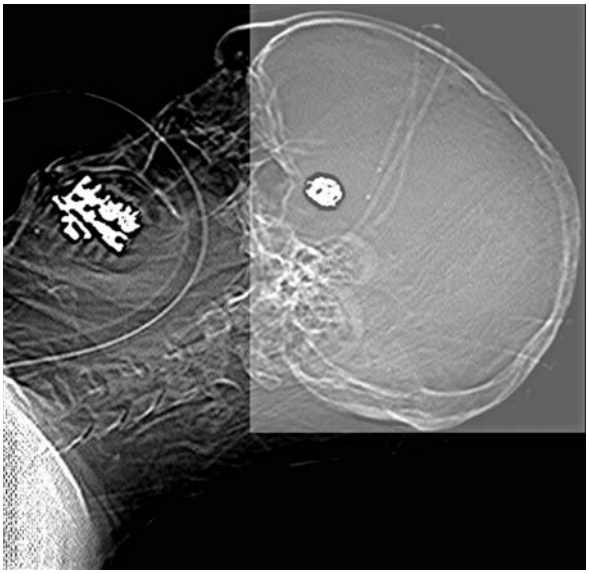

Fig. 1. Correct patient positioning for intracranial scans. Light box indicates the scan volume, the lenses of the eyes are outside the scan volume. Note the titanium coils after endovascular coil embolization of an aneurysm at the anterior communication artery

interpolation. Over-beaming depends on the diameter of the imaging beam, which correlates with the number of detectors used and the collimation. For instance, with a 64-detector-row scanner only the inner 20 detectors can be used for imaging; therefore a smaller beam is used, which reduces the area of over-beaming and over-ranging but increases the scan time.

Modern MDCT scanners allow long scan ranges to be covered with a single scan. This is advantageous for neurovascular CT, especially in stroke-imaging, as all supra-aortic arteries can be visualized from their origin at the aortic arch to the circle of Willis, including its branches. However, the easy availability and high quality of these long scan ranges make them tempting approaches for the coverage of longer scan ranges, as indicated for some individual diagnostic evaluations, but they result in an increased patient exposure. The scan ranges should always be individualized for the specific patient situation and limited to the diagnostically relevant area in order to protect radiation-sensitive organs such as the thyroid gland and lenses of the eye. If available, dose-modulation functions on the scanner side should always be used in cervical CTA to reduce the radiation dose at the upper and mid-cervical levels and to achieve an adequate dose at the lower cervical level, i.e., the shoulder region.

With modern MDCT scanners, the indications for sequential CT scanning, as opposed to spiral scanning, are limited to dynamic protocols, such as CT-perfusion (CTP), and to sequential scans of the infratentorial brain or skull base. Sequential scanning can reduce beam hardening artifacts and over-beaming; however, 3D refomation options are limited in sequential scanning.

For dynamic CTP, it is mandatory that any motion of the patient's head be prevented during the entire scanning period, either by explicit instructions to the patient or by effective fixation. For fixation in unconscious patients, large patches covering the forehead and the headrest are preferable to hook-and-loop fasteners and cushions. Sample scan parameters for CTP scanning are: tube voltage 80 kV; tube current 120–240 mAs; rotation time 1 s, scanning time 40–45 s, and a start delay of 6 s. To administer 40–50 ml of contrast agent at a flux of 5–10 ml/s, a central venous catheter or an 18-gauge injection needle at the cubital vein is mandatory. The quality of the arterial input function can be improved by using a saline pusher at the same injection speed directly after contrast agent administration.

Clinical Applications of Neurovascular MDCT

There are numerous applications and indications for neurovascular MDCT, including comprehensive stroke imaging, evaluation of the extra- and intracranial vasculature of the head and neck, as well as pre-operative therapy planning. In this chapter, we focus on the most commonly used and more specialized, but highly relevant, neurovascular MDCT applications.

Comprehensive Stroke Imaging

In most clinical settings, suspected ischemic or hemorrhagic stroke is the most frequent indication for emergency CT. CT is widely available and rapidly performed – advantages that are crucial in stroke, where "time is brain." Even though modern magnetic resonance (MR) imaging is a very valuable method to evaluate early stroke, only a small number of specialized radiology/neuroradiology departments offer stroke-MRI in a 24/7 time frame.

Historically, NECT was the only CT method available. However, even with MDCT, the evaluation of stroke always starts with standard NECT. NECT facilitates the differentiation of hemorrhagic from ischemic stroke and the exclusion of many other differential diagnoses. In a patient with subarachnoid hemorrhage (SAH), a subsequent in-

tracranial CTA should be performed (see "Intracranial Aneurysm") [16]. If no hemorrhage or other obvious reasons for stroke-like symptoms are identified and contraindications for the administration of contrast medium are absent, the next step is usually to obtain a CTA of the brain and neck.

After CTA and NECT have been carried out, it is important to evaluate any discrepancies between early stroke signs or visibly manifest infarction in NECT (Fig. 2) and the potential occlusions of vessels in CTA (Fig. 2b). It is therefore mandatory to check every segment of the intracranial arteries. Additional axial MIP reformations with a slice thickness of 5 mm and an increment of 1 mm can provide a very convenient and fast overview of all cerebral vessels [17]. Most commonly, thrombembolic occlusions can be found in one of the middle cerebral arteries (MCAs). In addition, potential hemodynamic stenoses or dissections need to be searched for. These are most commonly located in the proximal internal carotid artery (ICA) in close proximity to the carotid bulb (Fig. 3). Other common locations for relevant stenoses are the proximal portion of the common carotid artery and the distal, intracranial part of the ICA. Dissections are often located at the ICA and at the vertebral arteries.

If NECT shows that the extent of a cerebral infarction is less extensive than would be expected, given the territory of the occluded vessel, a perfusion analysis is indicated (step 3, Figs. 2, 3) [18, 19]. For CTP, sequential slices are acquired in cine mode during intravenous contrast injection, typically with a high flow rate of 5–10 ml/s and a scanning time of 40 s. CTP allows ischemic brain tissue ("tissue at risk", "penumbra") to be distinguished from infarction, thereby supporting therapeutic decision-making in regard to whether thrombolysis or mechanical recanalization is more beneficial to the patient.

Depending on the vendor of the scanner, two different mathematical reconstruction models are used for analyzing CTP, the maximum slope/gradient model (e.g., Siemens and Vitrea) and the deconvolution model (e.g., GE and Toshiba). Both models provide parameter maps of regional cerebral blood flow (rCBF) and regional cerebral blood volume (rCBV) and take into account either the time-to-peak (TTP, maximum slope model) or the mean-transit-time (MTT, deconvolution model).

In non-ischemic brain tissue, the CBF value is about 50–80 ml blood per 100 mg brain per minute. Flow reductions below 10–15 ml/100 mg/min usually lead to irreversible infarction after a few minutes. CBF values of 10–25 ml/100 mg/min tend to cause neurological dysfunction, but a complete recovery may occur if normal levels of perfusion are restored within hours or days. CBV values reflect the extent of regional autoregulation. rCBV is usually increased at the penumbra as a result of vasodilatation to compensate for a decrease in rCBF. Low or normal CBV values at regions with reduced CBF are normally predictive of irreversible infarction.

CTP can also aid in evaluating patients with new onset of stroke symptoms, or those with old infarctions or with multiple high-grade stenoses in different vessel territories (Fig. 4).

A new theoretical approach for estimating perfused blood volume from CTA and NECT volume data showed promising results in a recent study [20]; however, further evaluation of this technique is needed.

As an alternative to the above-mentioned protocol, the order of step 2 (CTA) and step 3 (CTP) can be reversed such that the time of the maximum contrast-enhancement peak of the CTP can be used as the scan delay of the CTA scan. This protocol is especially useful in scanners without automated bolus chasing/tracking techniques.

Carotid-Artery Stenosis

Atherosclerosis of the carotid artery is an important predisposing factor for ischemic stroke, and patients with high-grade stenosis of the carotid arteries are known to benefit from endarterectomy or stent-angioplasty. An exact determination of the degree of a carotid-artery stenosis is crucial for therapeutic decision-making [12]. In several studies, more reliable results were obtained using multidetector CTA (MD-CTA) than other imaging techniques [21-24].

To evaluate carotid artery stenoses with MD-CTA, the scan range should include the aortic arch and the circle of Willis, to ensure that stenoses at the origin of the common carotid artery (CCA), at the carotid bulb, and at the carotid siphon are reliably depicted (Fig. 4). To avoid streak artifacts due to high concentrations of contrast agent in the superior vena cava at the beginning of the injection, the use of a craniocaudal scan direction is recommended [25].

For image analysis, semi-automatic bone-segmentation/elimination algorithms can be employed (Fig. 5). Of the different approaches to bone elimination, the most commonly used algorithms rely on threshold-based region-growing techniques. These techniques can rapidly extract bone or vessels as long as there is a clear separation between the two structures, e.g., in the cervical part of the carotid arteries. The major disadvantage of this ap-

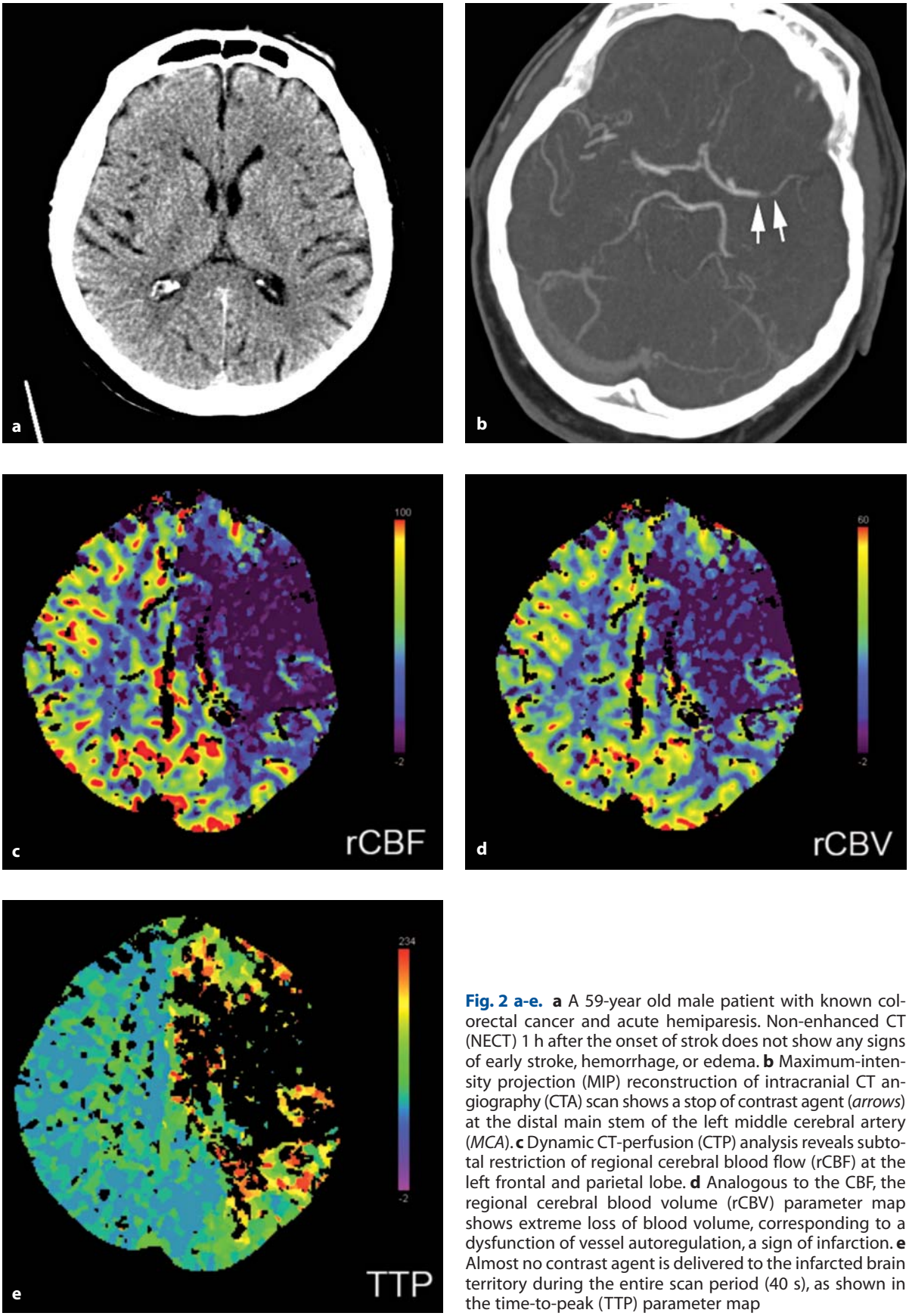

Fig. 2 a-e. **a** A 59-year old male patient with known colorectal cancer and acute hemiparesis. Non-enhanced CT (NECT) 1 h after the onset of strok does not show any signs of early stroke, hemorrhage, or edema. **b** Maximum-intensity projection (MIP) reconstruction of intracranial CT angiography (CTA) scan shows a stop of contrast agent (*arrows*) at the distal main stem of the left middle cerebral artery (*MCA*). **c** Dynamic CT-perfusion (CTP) analysis reveals subtotal restriction of regional cerebral blood flow (rCBF) at the left frontal and parietal lobe. **d** Analogous to the CBF, the regional cerebral blood volume (rCBV) parameter map shows extreme loss of blood volume, corresponding to a dysfunction of vessel autoregulation, a sign of infarction. **e** Almost no contrast agent is delivered to the infarcted brain territory during the entire scan period (40 s), as shown in the time-to-peak (TTP) parameter map

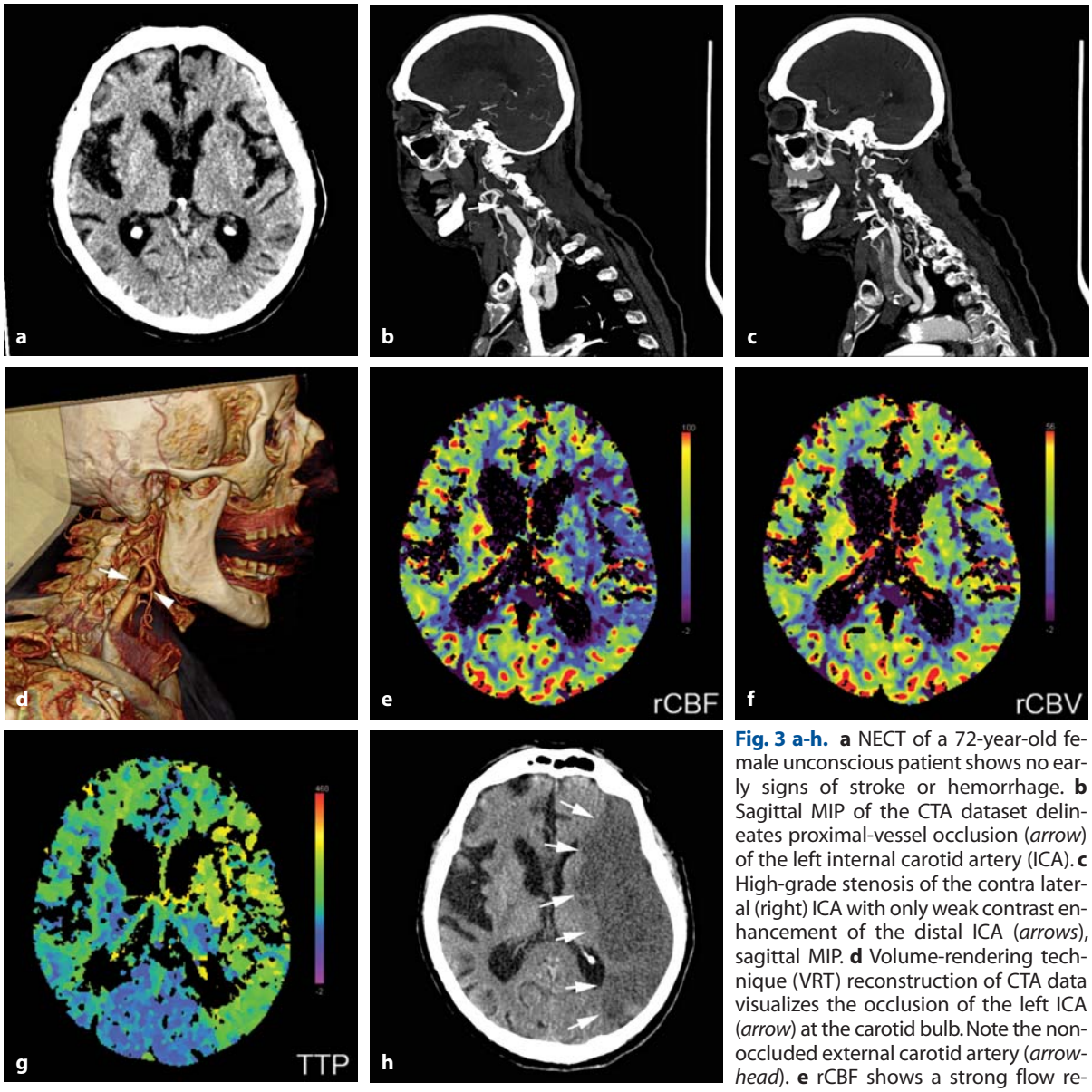

Fig. 3 a-h. **a** NECT of a 72-year-old female unconscious patient shows no early signs of stroke or hemorrhage. **b** Sagittal MIP of the CTA dataset delineates proximal-vessel occlusion (*arrow*) of the left internal carotid artery (ICA). **c** High-grade stenosis of the contra lateral (right) ICA with only weak contrast enhancement of the distal ICA (*arrows*), sagittal MIP. **d** Volume-rendering technique (VRT) reconstruction of CTA data visualizes the occlusion of the left ICA (*arrow*) at the carotid bulb. Note the non-occluded external carotid artery (*arrowhead*). **e** rCBF shows a strong flow restriction at the left MCA territory, CTP. **f** rCBV shows a mild reduction of blood volume at the left MCA territory, a sign of dysfunction in the autoregulation of the vessel and infarction. **g** TTP visualizes the prolonged contrast-agent delivery at left ICA territory and at the right (post-stenotic) ICA territory. No prolongation at the territories of the posterior cerebral arteries. **h** NECT follow-up 2 days after the onset of stroke shows complete infarction of the left MCA territory (*arrows*)

proach is that time-consuming manual corrections at the base of the skull are often necessary, as region-grow algorithms regularly fail in this region. In addition, the application of the algorithm to calcified plaques can result in excessive reduction of the residual lumen, thus exaggerating the degree of stenosis.

Alternatively, there are bone-subtraction algorithms that use either NECT volume data [13] or dual-energy material decomposition [8, 9] to subtract bone from the CTA data (Figs. 5, 6). After the segmentation process, cross-sectional MPR images perpendicular to the vessel can be aligned automatically using the centerline function of commercial vessel-analysis tools. Optional corresponding VRT reformations and stretched vessel images (MPR) can provide anatomic orientations (Fig. 4d). Manual or semi-automated measurements of the diameter or area of the vessel lumen can be made on the basis of these cross-sectional images. In the case of semi-automated

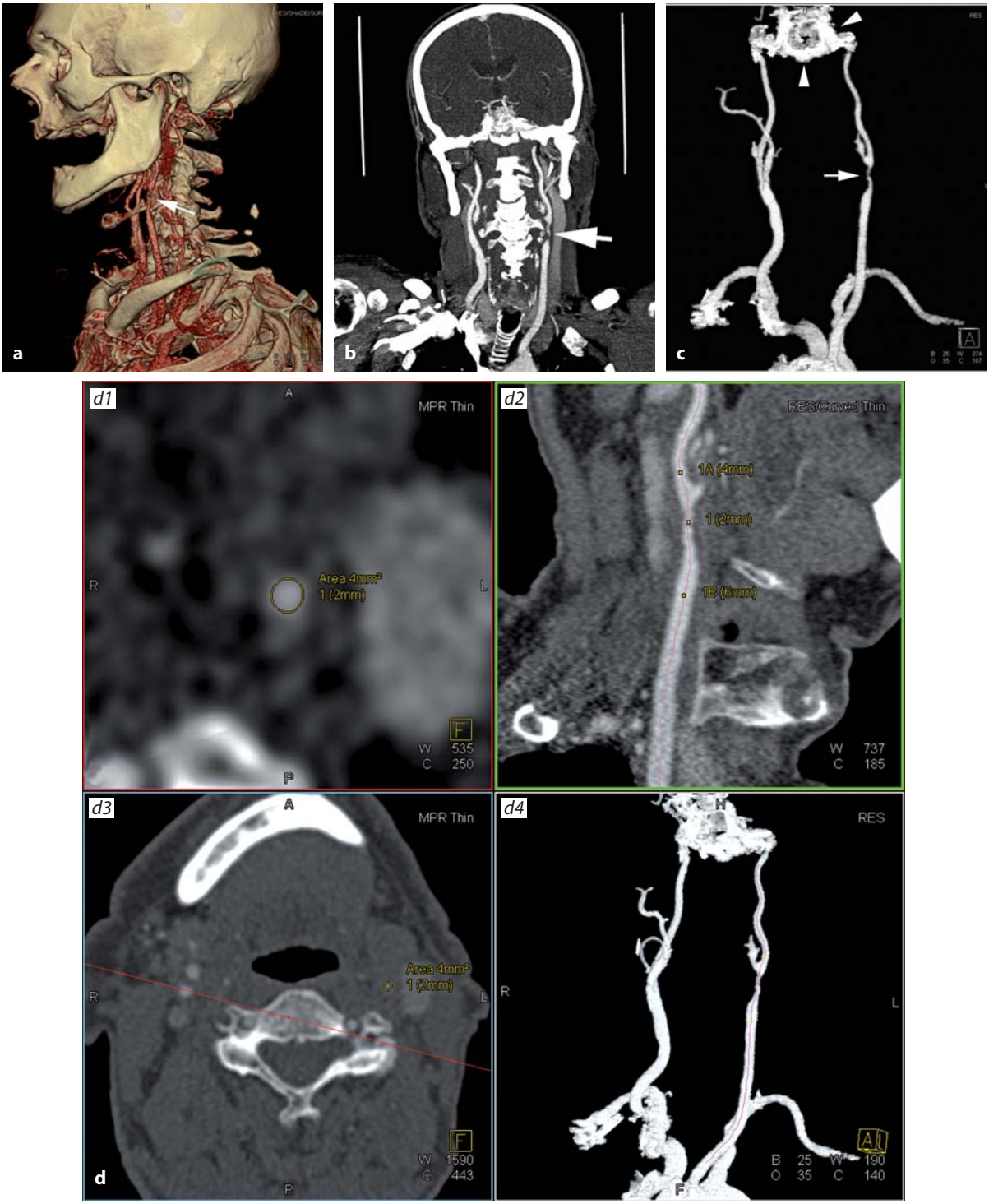

Fig. 4 a-d. **a** An 80-year-old male patient with high-grade stenosis at the left carotid bulb. VRT reconstruction of the CTA dataset clearly delineates the stenosis (*arrow*). **b** Coronal thin-MIP reconstruction provides more-detailed information about the stenosis (*arrow*). **c** Surface-rendering technique (SRT) reconstruction after regional-growth-based bone removal. Aortic arch, subclavian arteries, and extracranial carotid arteries remain visible. Vertebral arteries and distal segments of the external carotid artery have been removed by the bone-removal algorithm. Typical bone artifacts (*arrowheads*) at the infraclinoidal intracranial segments of both ICA after regional-growth bone removal. Stenosis of the left carotid bulb (*arrow*). **d** Computer-aided vessel analysis (Syngo Advanced Vessel Analysis, Siemens Medical Solutions, Erlangen, Germany). MPR reconstruction in axial orientation to the vessel with threshold-based diameter and area calculations of the vessel lumen (*d1*). Stretched MPR view of the traced vessel showing the entire vessel in one image; marks indicate user-driven quantifications (*d2*). Original axial CTA data (*d3*). SRT reconstruction after bone removal with vessel trace (*d4*)

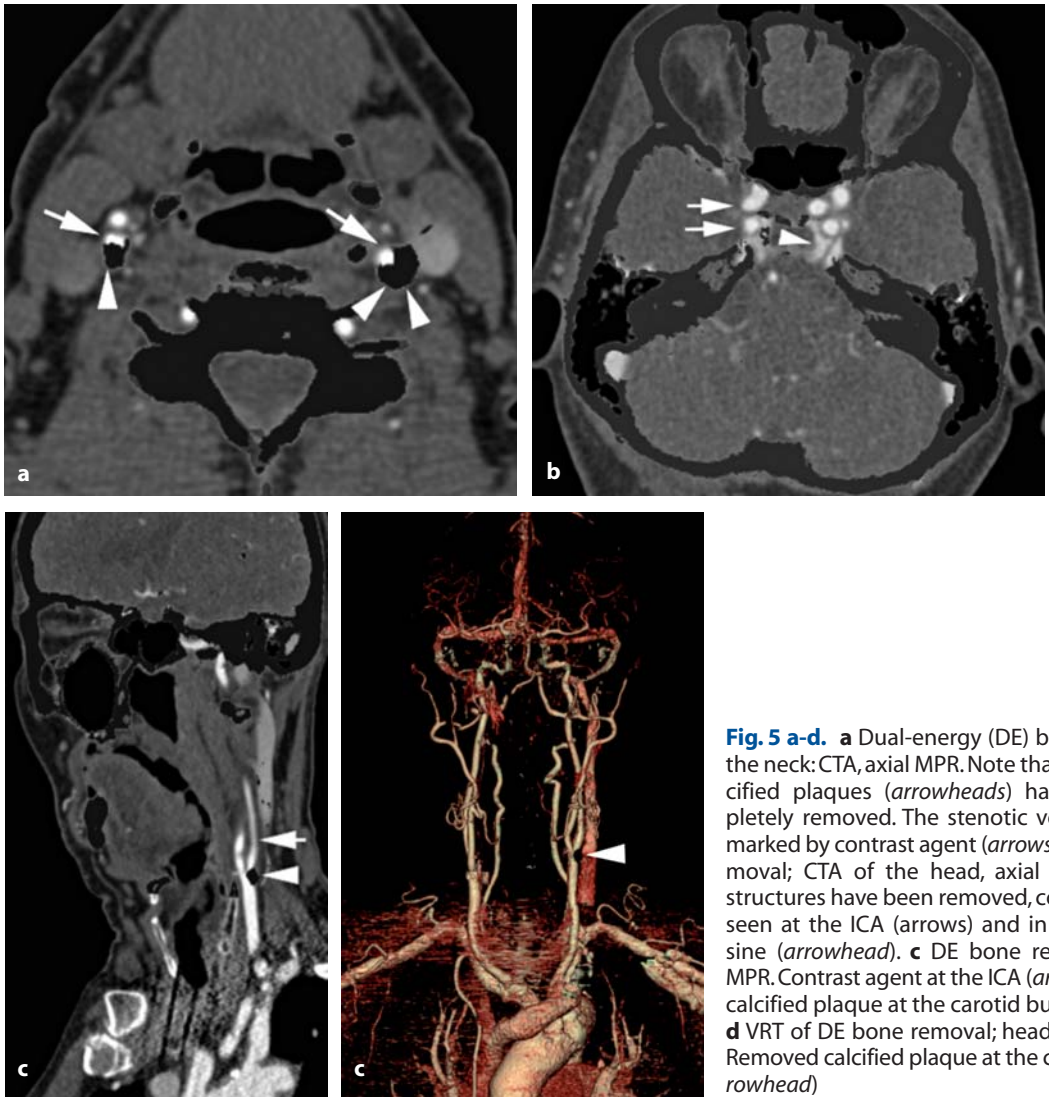

Fig. 5 a-d. **a** Dual-energy (DE) bone removal in the neck: CTA, axial MPR. Note that bone and calcified plaques (*arrowheads*) have been completely removed. The stenotic vessel is lumen-marked by contrast agent (*arrows*). **b** DE bone removal; CTA of the head, axial MPR. All bony structures have been removed, contrast agent is seen at the ICA (arrows) and in the cavernous sine (*arrowhead*). **c** DE bone removal: sagittal MPR. Contrast agent at the ICA (*arrows*), removed calcified plaque at the carotid bulb (*arrowhead*). **d** VRT of DE bone removal; head and neck CTA. Removed calcified plaque at the carotid bulb (*arrowhead*)

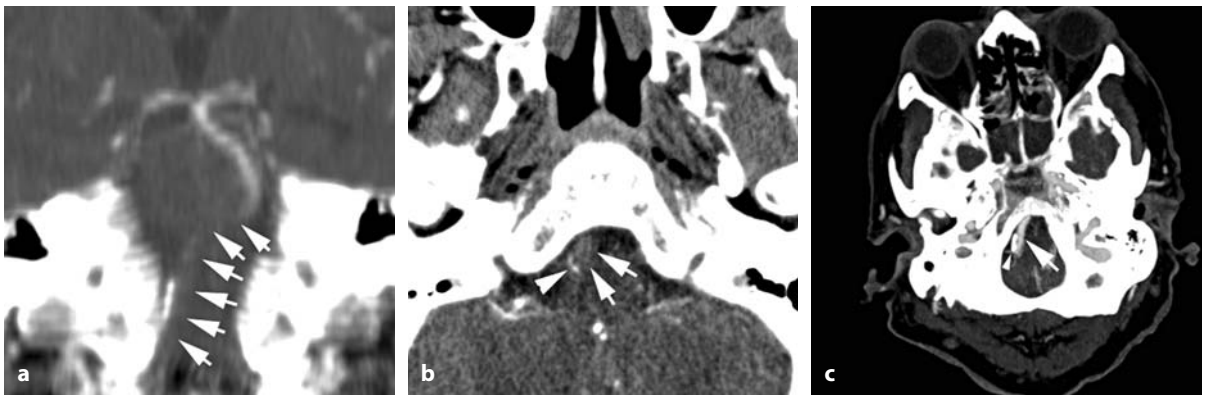

Fig. 6 a-c. **a** Basilar-artery (*BA*) thrombosis. Coronal MIP reconstruction of a 4-slice-CTA dataset showing normal contrast enhancement at the top and middle segments of the BA. Occluded lower BA and occluded V4 segment of the right vertebral artery (*VA*) (*arrows*). Note the calcified plaque at the VA. **b** Axial MPR at the level of the calcified plaque (*arrowhead*) shows that the V4- segment of the right VA is completely occluded by thrombus (*arrows*). **c** After thrombolysis, follow-up with 64-slice CTA shows complete recanalization of the formerly occluded V4 segment of the right VA (*arrow*); a high-grade stenosis at the level of the calcified plaque (*arrowhead*) remains

measurements, it is mandatory to check for common errors in lumen quantification, especially in the presence of branching or neighboring vessels, and boundary identification in the presence of calcifications [26].

Basilar-Artery Occlusions

Although the majority of cerebral infarctions are located in the territories of the internal carotid arteries, 20% of cerebral ischemic infarctions involve tissue supplied by the vertebrobasilar circulation. Occlusion of the basilar artery is a life-threatening condition whose usually unfavorable prognosis can only be improved by early detection and subsequent aggressive recanalization therapy [27].

In cases of suspected ischemia in the posterior circulation, CTA offers a swift and easy imaging modality to rule out pathologies of the vertebrobasilar arteries. The scan range should include the level of the second cervical vertebra in order to include the passage of the vertebral arteries (VAs) through the dura mater. In selected cases, a scan range including the entire vertebrobasilar circulation, beginning at the origin of the VAs at the subclavian arteries, provides additional information about potential pathologies of the VAs at the neck, such as dissections.

Additional sagittal and coronal or pseudo-coronal MIP reformations parallel to the clinoid provide excellent information about the basilar artery (Fig. 5). Additional VRT after bone subtraction may be useful to visualize stenoses.

Intracranial Aneurysm

Acute subarachnoid hemorrhage (SAH) following rupture of a cerebral aneurysm is associated with a high mortality. The incidence of intracranial aneurysm is thought to be about 1.9%. CTA can be used for the emergency evaluation of SAH in order to determine the appropriate neurosurgical or endovascular intervention for cerebral aneurysms and as a non-invasive screening modality for patients with a familial predisposition for developing intracranial aneurysms. While the gold-standard examination in SAH is still DSA, with modern MD-CTA techniques some authors now advocate MDCT as the method of choice to evaluate cerebral aneurysms [28, 29].

With the latest generation of MDCT it is possible to acquire CTA scans in an arterial phase without relevant contrast enhancement of the cerebral veins, thereby facilitating the evaluation of the intracavernous segments of the ICA. If available, bone subtraction is strongly recommended for evaluating the infraclinoid segments of the ICA [30]. When evaluating a CTA in a patient with SAH, it is helpful to perform cross-sectional sliding thin-slab MIP reformations (Fig. 7). In addition, VRT can be used for 3D visualization in therapy planning (Fig. 7).

In contrast to with the use of MDCT in the primary diagnosis of aneurysm, considerable challenges are posed by the follow-up of clipped or coiled aneurysms with CTA, as surgical clips or coils usually cause significant beam-hardening artifacts, thus altering the Hounsfield-unit values in the surrounding soft tissue and vessels [12].

Cerebral Venous Thrombosis

About 1% of all acute strokes or stroke-like events are caused by cerebral venous thrombosis (CVT). Thromboses can be located in the intracranial dural sinuses, the superficial cerebral veins, or in the deep cerebral veins.

On NECT, patients with CVT often demonstrate venous infarctions (50%) with cortical/subcortical petechial hemorrhages and edema. The “cord sign” (Fig. 8) reflects a more hyperdense dural sinus filled with thrombotic material. The “empty delta” or “empty triangle” sign (Fig. 8) refers to enhanced dura surrounding non-enhancing thrombus and can be found with CTA in 25–30% of patients with CVT.

The report of a CTA of the intracranial veins and sinuses needs to take into consideration that a large number of anatomic variants and arachnoidal granulations can mimic CVT.

Cerebral CT venography provides high-quality anatomic images of the intracranial venous circulation and can be used to rule out thrombosis and to pre-operatively map venous structures in patients with neoplasms [31]. CT venography is considered superior to MR venography in the identification of cerebral veins and dural sinuses and is at least equivalent in the diagnosis of dural-sinus thrombosis [32]. A scan delay of 30–35 s after contrast administration usually leads to combined arterial and venous contrast, which can be advantageous when the symptomatology of the patient is not clear-cut and arterial pathologies are included in the differential diagnosis.

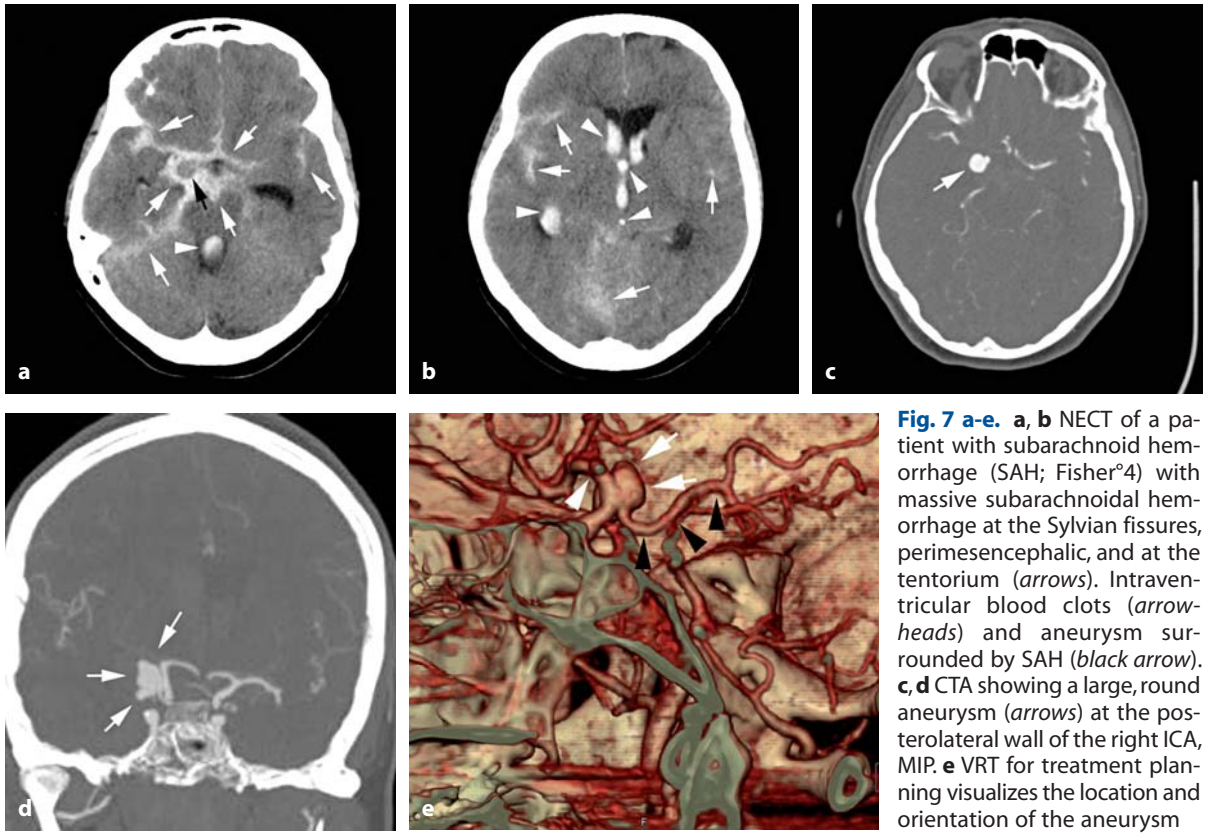

Fig. 7 a-e. **a**, **b** NECT of a patient with subarachnoid hemorrhage (SAH; Fisher°4) with massive subarachnoidal hemorrhage at the Sylvian fissures, perimesencephalic, and at the tentorium (*arrows*). Intraventricular blood clots (*arrowheads*) and aneurysm surrounded by SAH (*black arrow*). **c**, **d** CTA showing a large, round aneurysm (*arrows*) at the posterolateral wall of the right ICA, MIP. **e** VRT for treatment planning visualizes the location and orientation of the aneurysm

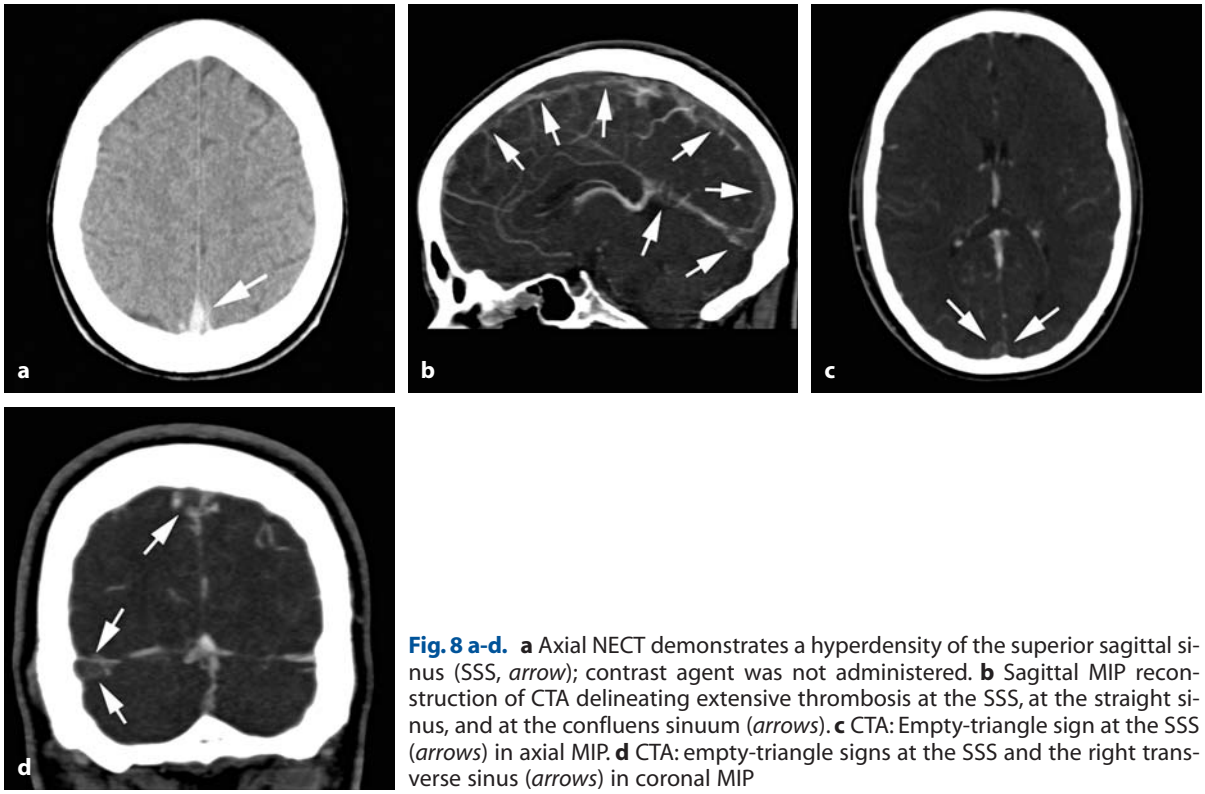

Fig. 8 a-d. **a** Axial NECT demonstrates a hyperdensity of the superior sagittal sinus (SSS, *arrow*); contrast agent was not administered. **b** Sagittal MIP reconstruction of CTA delineating extensive thrombosis at the SSS, at the straight sinus, and at the confluens sinuum (*arrows*). **c** CTA: Empty-triangle sign at the SSS (*arrows*) in axial MIP. **d** CTA: empty-triangle signs at the SSS and the right transverse sinus (*arrows*) in coronal MIP

References

1. Crawford CR, King KF (1990) Computed tomography scanning with simultaneous patient translation. Med Phys 17:967-982
2. Kalender WA, Seissler W, Klotz E, Vock P (1990) Spiral volumetric CT with single-breath-hold technique, continuous transport, and continuous scanner rotation. Radiology 176:181-183
3. Rubin GD, Dake MD, Semba CP (1995) Current status of three-dimensional spiral CT scanning for imaging the vasculature. Radiol Clin North Am 33:51-70
4. Napel S, Rubin GD, Jeffrey RB Jr (1993) STS-MIP: a new reconstruction technique for CT of the chest. J Comput Assist Tomogr 17:832-838
5. Flohr T, Bruder H, Stierstorfer K, Simon J, Schaller S, Ohnesorge B (2002) New technical developments in multislice CT, part 2: sub-millimeter 16-slice scanning and increased gantry rotation speed for cardiac imaging. Rofo 174:1022-1027
6. Flohr T, Stierstorfer K, Bruder H, Simon J, Schaller S (2002) New technical developments in multislice CT-Part 1: Approaching isotropic resolution with sub-millimeter 16-slice scanning. Rofo 174:839-845
7. Ertl-Wagner BB, Bruening R, Blume J, Hoffmann RT, Snyder B, Herrmann KA, Reiser MF (2005) Prospective, multireader evaluation of image quality and vascular delineation of multislice CT angiography of the brain. Eur Radiol 15:1051-1059
8. Flohr TG, McCollough CH, Bruder H, Petersilka M, Gruber K, Suss C, Grasruck M, Stierstorfer K, Krauss B, Raupach R, Primak AN, Kuttner A, Achenbach S, Becker C, Kopp A, Ohnesorge BM (2006) First performance evaluation of a dual-source CT (DSCT) system. Eur Radiol 16:256-268
9. Johnson TR, Krauss B, Sedlmair M, Grasruck M, Bruder H, Morhard D, Fink C, Weckbach S, Lenhard M, Schmidt B, Flohr T, Reiser MF, Becker CR (2006) Material differentiation by dual energy CT: initial experience. Eur Radiol
10. Anderson GB, Steinke DE, Petruk KC, Ashforth R, Findlay JM (1999) Computed tomographic angiography versus digital subtraction angiography for the diagnosis and early treatment of ruptured intracranial aneurysms. Neurosurgery 45:1315-1320; discussion 1320-1312
11. Chappell ET, Moure FC, Good MC (2003) Comparison of computed tomographic angiography with digital subtraction angiography in the diagnosis of cerebral aneurysms: a meta-analysis. Neurosurgery 52:624-631; discussion 630-621
12. Lell MM, Anders K, Uder M, Klotz E, Ditt H, Vega-Higuera F, Boskamp T, Bautz WA, Tomandl BF (2006) New techniques in CT angiography. Radiographics 26 Suppl 1:S45-62
13. Tomandl BF, Hammen T, Klotz E, Ditt H, Stemper B, Lell M (2006) Bone-subtraction CT angiography for the evaluation of intracranial aneurysms. AJNR Am J Neuroradiol 27:55-59
14. Hoh BL, Cheung AC, Rabinov JD, Pryor JC, Carter BS, Ogilvy CS (2004) Results of a prospective protocol of computed tomographic angiography in place of catheter angiography as the only diagnostic and pretreatment planning study for cerebral aneurysms by a combined neurovascular team. Neurosurgery 54:1329-1340; discussion 1340-1322
15. Ertl-Wagner BB, Hoffmann RT, Bruning R, Herrmann K, Snyder B, Blume JD, Reiser MF (2004) Multi-detector row CT angiography of the brain at various kilovoltage settings. Radiology 231:528-535
16. Tomandl BF, Klotz E, Handschu R, Stemper B, Reinhardt F, Huk WJ, Eberhardt KE, Fateh-Moghadam S (2003) Comprehensive imaging of ischemic stroke with multisection CT. Radiographics 23:565-592
17. Ertl-Wagner BB, Bruening R, Blume J, Hoffmann RT, Mueller-Schunk S, Snyder B, Reiser MF (2006) Relative value of sliding-thin-slab multiplanar reformations and sliding-thin-slab maximum intensity projections as reformatting techniques in multisection CT angiography of the cervicocranial vessels. AJNR Am J Neuroradiol 27:107-113
18. Wintermark M (2005) Brain perfusion-CT in acute stroke patients. Eur Radiol 15 Suppl 4:D28-31
19. Kloska SP, Nabavi DG, Gaus C, Nam EM, Klotz E, Ringelstein EB, Heindel W (2004) Acute stroke assessment with CT: do we need multimodal evaluation? Radiology 233:79-86
20. Kloska SP, Fischer T, Nabavi DG, Dittrich R, Ditt H, Klotz E, Fischbach R, Ringelstein EB, Heindel W (2007) Color-coded perfused blood volume imaging using multidetector CT: initial results of whole-brain perfusion analysis in acute cerebral ischemia. Eur Radiol 17:2352-2358
21. Clevert DA, Johnson T, Jung EM, Clevert DA, Flach PM, Strautz TI, Ritter G, Gallegos MT, Kubale R, Becker C, Reiser M (2007) Color Doppler, power Doppler and B-flow ultrasound in the assessment of ICA stenosis: Comparison with 64-MD-CT angiography. Eur Radiol 17:2149-2159
22. Hacklander T, Wegner H, Hoppe S, Danckworth A, Kempkes U, Fischer M, Mertens H, Caldwell JH (2006) Agreement of multislice CT angiography and MR angiography in assessing the degree of carotid artery stenosis in consideration of different methods of postprocessing. J Comput Assist Tomogr 30:433-442
23. Silvennoinen HM, Ikonen S, Soinne L, Railo M, Valanne L (2007) CT angiographic analysis of carotid artery stenosis: comparison of manual assessment, semiautomatic vessel analysis, and digital subtraction angiography. AJNR Am J Neuroradiol 28:97-103
24. Ertl-Wagner B, Bruning R, Hoffmann RT, Meimarakis G, Reiser MF (2004) [Diagnostic evaluation of carotid artery stenoses with multislice CT angiography. Review of the literature and results of a pilot study]. Radiologe 44:960-966

25. de Monye C, de Weert TT, Zaalberg W, Cademartiri F, Siepman DA, Dippel DW, van der Lugt A (2006) Optimization of CT angiography of the carotid artery with a 16-MDCT scanner: craniocaudal scan direction reduces contrast material-related perivenous artifacts. AJR Am J Roentgenol 186:1737-1745
26. Bucek RA, Puchner S, Kanitsar A, Rand T, Lammer J (2007) Automated CTA quantification of internal carotid artery stenosis: a pilot trial. J Endovasc Ther 14:70-76
27. Pfefferkorn T, Mayer TE, Schulte-Altedorneburg G, Bruckmann H, Hamann GF, Dichgans M (2006) [Diagnosis and therapy of basilar artery occlusion]. Nervenarzt 77:416-422
28. Tipper G, JM UK-I, Price SJ, Trivedi RA, Cross JJ, Higgins NJ, Farmer R, Wat J, Kirollos R, Kirkpatrick PJ, Antoun NM, Gillard JH (2005) Detection and evaluation of intracranial aneurysms with 16-row multislice CT angiography. Clin Radiol 60:565-572
29. Villablanca JP, Jahan R, Hooshi P, Lim S, Duckwiler G, Patel A, Sayre J, Martin N, Frazee J, Bentson J, Vinuela F (2002) Detection and characterization of very small cerebral aneurysms by using 2D and 3D helical CT angiography. AJNR Am J Neuroradiol 23:1187-1198
30. Morhard D, Fink C, Nikolaou K, Johnson T, Becker C, Reiser M (2007) 64-slice CT angiography (CTA) of the head: efficacy of improved automated bone-subtraction algorithm. In: ECR 2007. Vienna, Austria
31. Casey SO, Alberico RA, Patel M, Jimenez JM, Ozsvath RR, Maguire WM, Taylor ML (1996) Cerebral CT venography. Radiology 198:163-170
32. Ozsvath RR, Casey SO, Lustrin ES, Alberico RA, Hassankhani A, Patel M (1997) Cerebral venography: comparison of CT and MR projection venography. AJR Am J Roentgenol 169:1699-1707